ICARUS 88, 87–96 (1990)

Ethane Abundance on Neptune

THEODOR KOSTIUK[1] AND FRED ESPENAK

Planetary Systems Branch, Laboratory for Extraterrestrial Physics, NASA Goddard Space Flight Center, Greenbelt, Maryland 20771

PAUL ROMANI[2]

Science Systems and Applications, Inc., Seabrook, Maryland 20706

DAVID ZIPOY[1]

Astronomy Program, University of Maryland, College Park, Maryland 20742

AND

JEFF GOLDSTEIN[1]

Laboratory for Astrophysics, National Air and Space Museum, Washington, D.C. 20560

Received October 5, 1989; revised June 4, 1990

Ethane mole fractions on Neptune were determined from infrared heterodyne spectroscopic measurements of the C_2H_6 RR (4,5) emission line at 840.9764 cm^{-1}. The measured line was fit using existing atmospheric models and C_2H_6 mixing ratio profiles for Neptune. The value of the ethane mole fraction retrieved, using a profile consisting of a constant mixing ratio with altitude above the saturation region, was lower than that obtained by G. S. Orton *et al.* (1987, *Icarus* 70, 1–12), but was within the 2σ error bounds of their results. Nonconstant mixing ratio profiles derived from the photochemical model of P. N. Romani and S. K. Atreya (1989, *Geophys. Res. Lett.* 16, 941–944) were also tested. Our results require 2.0 to 5.8 times more ethane in the 0.02–2 mbar pressure region than the model predicts. Ethane mole fractions $\sim 3 \times 10^{-6}$ were retrieved near the 0.27-mbar pressure level (line center contribution function peak) for all models tested. The cumulative uncertainty on the retrievals, excluding that associated with the temperature profile, is 30%. Better agreement with the model can be achieved if the eddy mixing is reduced in the lower stratosphere and/or the stratospheric temperature is increased by >10 K above the 6-mbar level.

INTRODUCTION

Ethane (C_2H_6) was first detected in infrared emission from Neptune by Macy and Sinton (1977) and by Gillett and Rieke (1977). Gillett and Rieke reported a mixing ratio Q of about 5×10^{-7}. Macy (1980) derived an abundance relative to H_2 of $\sim 10^{-6}$, with an uncertainty of a factor of 5. Orton *et al.* (1983) obtained a mixing ratio of 3×10^{-6}. More recently Orton *et al.* (1987) deduced an ethane mixing ratio on Neptune of 6×10^{-6} with a total uncertainty factor of 3.2. Recent recalibration of their data (Orton *et al.* 1990) has not changed their retrieved mean C_2H_6 mixing ratio.

Orton *et al.* (1987) used a constant mixing

[1] Visiting astronomer at the Infrared Telescope Facility, which is operated by the University of Hawaii under contract from the National Aeronautics and Space Administration.

[2] Also at Planetary Systems Branch, Laboratory for Extraterrestrial Physics, NASA Goddard Space Flight Center, Greenbelt, MD 20771.

0019-1035/90 $3.00

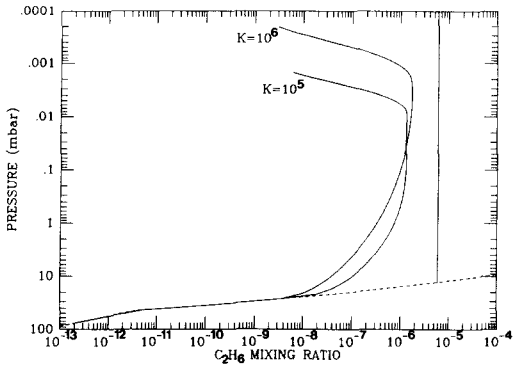

FIG. 1. Ethane mixing ratio profiles for Neptune. The constant mixing profile used by Orton *et al.* (1987) with $Q = 6 \times 10^{-6}$ above the saturation curve (dashed line) is shown along with the $K = 10^5$ and $K = 10^6$ mixing profiles derived from their photochemical model by Romani and Atreya (1989). Note that the lower eddy mixing coefficient model increases the C_2H_6 abundance in the lower stratosphere, where the observed lines are formed. The shapes of these profiles were used to fit our observed spectrum.

ratio profile in the upper stratosphere down to the saturation level in the lower stratosphere, below which it followed the saturation mixing ratio profile (see Fig. 1). Numerical models of methane photochemistry on Neptune that include a condensation loss for ethane (Romani and Atreya 1989) predict more realistic nonconstant ethane mixing ratio profiles above the condensation level. The model profiles given in Fig. 1 are based upon an assumed 2% methane (CH_4) stratospheric mixing ratio. Ethane is produced from methane photolysis near the microbar pressure level. It is then transported downward to its condensation level. The resultant ethane mixing ratios (mole fractions) remain less than 2×10^{-6}. The extent of depletion of C_2H_6 above the condensation layer is determined by the strength of eddy mixing in the lower stratosphere. This is illustrated in Fig. 1, where cases for two different values of the eddy diffusion coefficient, K (10^5 and 10^6 cm^2 sec^{-1}), at the CH_4 homopause are presented. In both cases K was assumed to be proportional to the inverse square root of the atmospheric number density.

Infrared observations on Neptune to date were made at relatively low spectral resolution (resolving powers < 100), measuring only broad molecular band structure with peak intensities diluted by the low resolving power. Such spectra can also be strongly affected by the shape of the underlying molecular and aerosol continuum contributions. Measurement of single emission lines (e.g., ethane in the 12-μm ν_9 band) would yield higher brightness temperatures, representative of the region of line formation. Such measurements are not subject to possible confusion with spectra from other constituents and are weakly affected by changes in the continuum. Thus analysis of the line profiles should retrieve more precise values for ethane abundance, as was demonstrated in the case of Jupiter (Kostiuk *et al.* 1983, 1987).

We report here on the measurement of the ethane ν_9 RR($K = 4$, $J = 5$) emission line doublet at 840.9764 cm^{-1} from Neptune using infrared heterodyne spectroscopy with a spectral resolving power $>10^5$. Ethane abundances retrieved from the observed data were compared to the most recent observational results obtained by Orton *et al.* (1987) and were used to test the combined photochemical-condensation models developed by Romani and Atreya (1989) (see Fig. 1).

OBSERVATIONS

Measurements were made May 29–June 1, 1989 at the NASA Infrared Telescope Facility on Mauna Kea, Hawaii. The instrumental diffraction limited field-of-view at 12 μm was $\sim$1 arcsec full-width-at-half-maximum (FWHM). Neptune's angular diameter was 2.28 arcsec at the time of the observations. The center of the planetary image from a visible tracking system (incorporating an intensified television camera and monitor) was actively maintained on reference crosshairs conjugate to the heterodyne detector/mixer. The reference crosshairs were aligned with the detector position using several reference stars. From the stellar

images, visible seeing was estimated to be ~0.5 arcsec. The infrared seeing is significantly better. Combining the instrumental field-of-view, infrared seeing, and our rms tracking errors (~0.5 arcsec) in quadrature yields an effective beam on Neptune approximated by a Gaussian profile with a FWHM of 1.2 arcsec. This indicates that emission from the entire planetary disc contributed to the measured spectrum as discussed below. The measured signal was calibrated using the Moon and a calibrated blackbody reference. The resultant uncertainty in Neptune's absolute radiance was less than 10%. This translates into ≤1 K uncertainty in the retrieved brightness temperature and ~15% maximum uncertainty in the final mole fraction retrieval. The infrared heterodyne spectrometer and the measurement technique are described in Kostiuk and Mumma (1983), Kostiuk *et al.* (1987), and Kostiuk *et al.* (1989).

The results of the observations (~5.5 hr of integration) are presented in Fig. 3. Radiance and single-sideband brightness temperature are plotted versus frequency relative to the RR (4,5) line center position. Each step in the histogram corresponds to 100 MHz (0.0033 cm^{-1}), except the two extreme right steps, which correspond to 150 and 125 MHz, respectively. The total instrumental bandwidth is 1600 MHz (0.053 cm^{-1}). Also given in the figure is the frequency position (841.0007 cm^{-1}) of the P30 line of the $^{14}C^{16}O_2$ laser local oscillator (LO). The data in the first 100 MHz from the LO is lost due to relative shifting of the individual 7-min scans, which compose the resultant spectrum. These data shifts are necessary to account for changes in the frequency position of the measured lines due to the changing line-of-sight velocity of Neptune over the period of integration (5.5 hr over 3 days). The markers on the abscissa are positions of ethane lines. These lines are all doublets (~0.003 cm^{-1} separation) formed by torsional splitting (Susskind *et al.* 1982). Line rest frequencies and absolute intensities at 296 K were taken from Daunt *et al.* (1984). The frequency of the stronger RR(4,5) line, 840.9764 cm^{-1}, corresponds to the "0" on the frequency scale.

RESULTS

To compare our measurements to existing data, the line spectrum from Neptune in our instrumental bandwidth was calculated from a solution of the radiative transfer equation using a 32-layer atmosphere extending between the 100- and 0.001-mbar pressure levels, and an appropriate thermal structure and ethane mixing profile. Line intensities at 296 K used for the C_2H_6 RR(4,5) lines were 0.016 and 0.004 cm^{-2} atm^{-1}, with an uncertainty of ~10% (Daunt *et al.* 1984). The known lower state energies and a rotational partition function temperature dependence of $T^{-3/2}$ were used to scale the line intensities to the temperature at each atmospheric layer.

The signal detected by the spectrometer depends on the distribution of emitted intensity across Neptune's disc, the seeing/tracking profile (beam dilution) on the planet, and on the instrumental field-of-view due to the heterodyne sensitivity distribution of the detector/mixer matched to the diffraction limit of the telescope optics (1 arcsec FWHM on the source). The ethane emission lines are nearly optically thin, thus a significant contribution to the total planetary stratospheric emission comes from the outer limbs of the planetary disc (2.28-arcsec diameter). The amount of this limb contribution to our detected signal is increased by the Gaussian seeing/tracking profile on the planet. It is reduced by the heterodyne detector sensitivity profile which can be assumed to be a Gaussian matched to the 1-arcsec diffraction limit and truncated at the detector edge (equivalent to 2-arcsec diameter on the source). The resultant convolution of these three effects is equivalent to a mean representative viewing angle of 47°. The line spectrum was calculated using this viewing angle. An uncertainty of ±5° results from the uncertainty in the heterodyne sensitivity profile of the detector and seeing/tracking

profile. This corresponds to +7, −12 percent variation in the retrieved C_2H_6 mole fractions.

The calculated spectrum was convolved with a broadening function, resulting from the range of velocities in our field-of-view due to Neptune's rotation, weighted by the effective beam distribution on the planet. Taking Neptune's period of rotation to be 17.7 hr (Hammel 1989), line broadening of ~210 MHz (FWHM) is expected within our field-of-view. This value of the rotation period is within the range determined from recent Voyager 2 Imaging Science results (16–18.3 hr; Smith *et al.* 1989) and within 10% of the period determined from planetary radio emission (16.11 hr; Warwick *et al.* 1989). The width of the line broadening function is inversely proportional to the period of rotation and a 10% variation in the rotation period results in a 6% increase in the retrieved C_2H_6 mole fractions.

Three different input mixing ratio profiles were tested using our data, a constant mole fraction above the condensation level (as used by Orton *et al.* 1987), and the profiles from the $K = 10^5$ and $K = 10^6$ cases of Romani and Atreya (1989). The optimal mixing ratio profiles were obtained by scaling the input profiles by a factor constant with altitude in an iterative procedure until a best fit to our observations was obtained (see Kostiuk *et al.* 1983, 1987). Results of such fits are given below. In all cases the contribution functions for the RR (4,5) line peaked between the 0.2- and-2 mbar levels.

Constant mixing profile. To compare to the Orton *et al.* (1987) result, their retrieved constant mixing profile for C_2H_6 of 6×10^{-6} (Fig. 1) and their temperature profile shown in Fig. 2 (G. S. Orton, 1989, personal communication, Jet Propulsion Laboratory, California Institute of Technology, Pasadena) were used to calculate the modeled spectrum shown in Fig. 3. The best fit solution to our data (mole fraction $Q_{fit} = 3.0 \times 10^{-6}$) is also shown in Fig. 3. The σ of the fit is also given. A precision of 20% on the retrieved mixing profile was established by introducing random noise of the same σ on the best fit solution and fitting the new "data" with the atmospheric model. Ten such fits were generated and the standard deviation from the mean is the determined uncertainty. Although our result indicates 50% lower C_2H_6 abundance than the mean retrieved by Orton *et al.* (1987, 1990), the value is within two of their standard deviations.

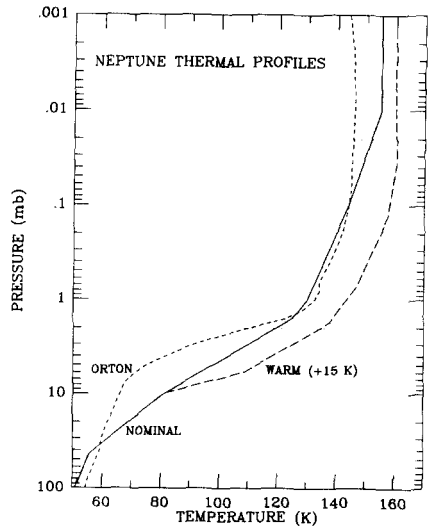

FIG. 2. The three thermal profiles used in retrieving the ethane mole fraction on Neptune. The horizontal dotted lines mark off the region of C_2H_6 line formation as illustrated by the weighting functions (see Fig. 6). The Nominal profile is the Appleby profile given in Tokunaga *et al.* (1983) and was used in the photochemical model and in fitting the photochemical model to our data. The Orton profile is from Orton *et al.* (1987), supplied by G. Orton. This was used in comparing our observations to Orton *et al.* (1987). The warm profile (dashed curve) represents a 15 K increased temperature profile (from 6 to 0.03 mbar). This warm profile provided the best fit to our data using the $K = 10^5$ mixing profile.

$K = 10^6$ mixing profile. The data were also fit using the more realistic mixing profiles derived from the combined condensation and photochemical models of Romani and Atreya (1989) shown in Fig. 1. We used the same temperature–pressure profile in our radiative transfer calculations and modeling of the C_2H_6 spectrum as was used in the

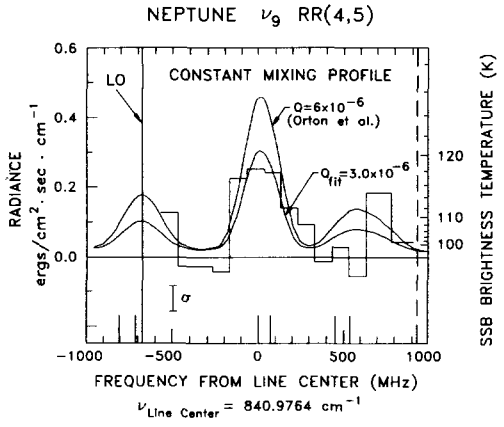

FIG. 3. The measured ethane spectrum (histogram) and best fit to the measurements (Q_{fit} = 3.0 ± 0.6 × 10^{-6}) using the constant mixing profile are shown. The spectrum calculated using the value retrieved by Orton *et al.* (1987), Q = 6 × 10^{-6}, is also shown for comparison.

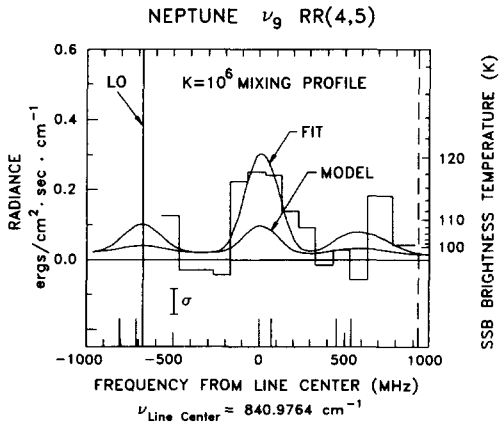

FIG. 4. Comparison of the spectrum calculated using the K = 10^6 mixing profile model of Romani and Atreya (1989) and the best fit to the observations (4.5 × the model).

photochemical model (Romani and Atreya 1989). The profile is given in Fig. 2. It comes from theoretical calculations by J. F. Appleby as given in Fig. 3 of Tokunaga et al. (1983). This profile lies in between curves d and c in Fig. 5 of Appleby (1986) in the pressure region where our contribution functions peaks (0.2–2 mbar). So it is a "warm" Appleby profile with only curve c being warmer by about 10 K.

The spectrum calculated using the model with K = 10^6 cm^2 sec^{-1} at the methane homopause is plotted in Fig. 4. The spectrum is compared to our observed data and the best fit spectrum. The model mixing (mole fraction) profile is ~4.5 times lower than that obtained from the best fit to the data (also shown in Fig. 4). An ethane mole fraction of Q = 3.0 × 10^{-6} at the 0.27-mbar pressure level (line center contribution function peak) was retrieved. The precision uncertainty in the results was determined as in the constant mixing profile case and is also ~20%.

K = 10^5 mixing profile. The calculated model spectrum and best fit spectrum for the K = 10^5 cm^2 sec^{-1} mixing profile model of Romani and Atreya (1989) are presented in Fig. 5. The retrieved mole fraction profile for C_2H_6 is ~2.8 times the model profile. An ethane mole fraction of ~3.3 × 10^{-6} at 0.27 mbar (line center contribution function peak) was retrieved. The precision of the retrieval is again ~20%. Figure 6 illustrates the temperature profile used, the resultant mixing profile and the contribution func-

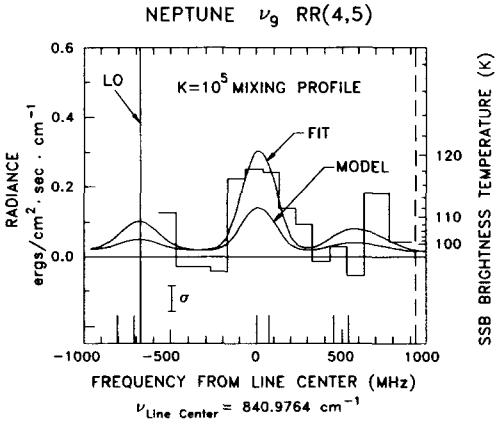

FIG. 5. Comparison of the spectrum calculated using the K = 10^5 mixing profile model of Romani and Atreya (1989) and the best fit to the observations (2.8 × the model). Note that the lower eddy mixing yields a somewhat better agreement with the data (compare to Fig. 4).

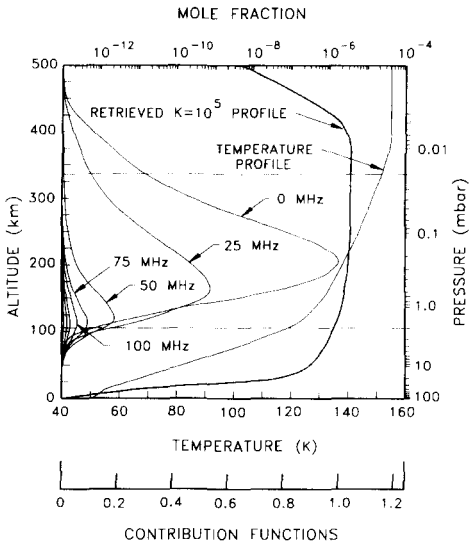

FIG. 6. The retrieved C_2H_6 mixing profile using the $K = 10^5$ model shape in the iterative fitting routine. The retrieved mole fractions were 2.8 times greater at all altitudes than the model of Romani and Atreya (1989). The calculated contribution functions and temperature profile used are also given. Note that the contribution functions and, hence, the observations cover predominantly the 0.02 to 2 mbar pressure region.

tions. The pressure region probed lies between about 0.02 and 2 mbar. This range of pressures is similar in all three retrievals described here.

DISCUSSION

Uncertainties. The various sources of uncertainties and their cumulative effect on the retrieved C_2H_6 mole fraction are now discussed. We distinguish between the uncertainty associated with the ability to fit the data with a given set of input parameters (precision) and the uncertainty due to the input parameters (accuracy). As was described earlier, our precision is 20%. The accuracy is dependent on the effect of absolute intensity calibration (~15% uncertainty on the mole fraction retrieved), the knowledge of the true ethane molecular line intensities (10%), the uncertainty in the mean viewing angle (~10%), and the knowledge of the period of rotation of Neptune (6%). The cumulative accuracy uncertainty due to these uncorrelated and (assumed) random errors is 21%. In the worst case, if the errors add directly, a 41% accuracy uncertainty can be expected. Including the precision uncertainty, a 30% error limit on the retrieved mole fractions is obtained, with the worst case uncertainty of 45%. The lack of knowledge of the true atmospheric model (temperature profile) introduces a much greater accuracy uncertainty. This uncertainty can be greater than a factor of two (see Temperature section below).

Eddy mixing effects. These observational results, as a test of the photochemical model (Romani and Atreya 1989), indicate that the model produces too little ethane. One possible way to reconcile the model with the observations is to lower the eddy mixing coefficient in the model in the lower stratosphere (e.g., for the case where $K = 10^5$ cm^2 sec^{-1} at the methane homopause, $K \sim 10^4$ cm^2 sec^{-1} in the C_2H_6 line formation region). There are two sources of ethane in the photochemical models. The first is from direct photolysis of methane which peaks where an optical depth of unity is reached in the strong solar Lyman-α line due to CH_4 absorption (μbar level). Eddy diffusion then transports the C_2H_6 down to its condensation sink to ice crystals near the temperature minimum. The second source occurs if the column density of acetylene (C_2H_2) becomes large enough so that an optical depth of unity is reached in C_2H_2 absorption at wavelengths beyond the methane cutoff at 1500 Å. Due to both the lower absorption cross sections and lower relative abundance of C_2H_2 compared to CH_4, this occurs in the millibar pressure region. The photolysis of C_2H_2 can catalytically convert CH_4 to C_2H_6. For the upper stratospheric source of ethane (CH_4 photolysis), lowering the eddy diffusion coefficient in the lower stratosphere (millibar region) increases the ethane mixing ratio there. This is because the column chemical production rate of C_2H_6 remains relatively unchanged, so the downward flux must remain constant. If K goes down then

the mixing ratio in the lower stratosphere must increase to keep the downward flux the same. Not only is the ethane mixing ratio increased, but so is the C_2H_2 mixing ratio, for the same reasons. This increase in C_2H_2 can then make the second mechanism for the production of C_2H_6 more significant. A photochemical model developed by Strobel and Summers (M. E. Summers, 1989, personal communication, Naval Research Laboratory, Washington, DC) with lower K's than used here shows a two-fold increase in the C_2H_6 mixing profile in the lower stratosphere.

The ethane mixing profiles on Neptune derived from our line measurements yield values considerably greater (2.0–5.8 times) than the theoretical models predict. Better agreement is obtained with the lower eddy mixing coefficient model ($K = 10^5$). Since the measurements are sensitive to emission from the 0.02- to 2-mbar pressure region (see Fig. 6), as was discussed above, greater reduction of K there would increase the ethane abundance even more and provide closer agreement. The requirement of lower eddy mixing coefficients in the lower stratosphere of Neptune is, therefore, consistent with our retrievals.

Preliminary analysis of the Voyager 2 Ultraviolet Spectrometer (UVS) data suggests an eddy mixing coefficient on the order of 3×10^7 at the methane homopause (Broadfoot *et al.* 1989). Although higher than the values used here, this result does not conflict with our conclusion, since the UVS data pertain to the microbar pressure region on Neptune, while the present arguments address primarily the region near 1 mbar.

Temperature. The retrieved ethane abundances are greatly dependent on the temperature–pressure profile used in the analysis. A much warmer temperature profile in the line formation region of Neptune's stratosphere may help to reconcile the differences between the model and the observations. This would not only increase the emission per molecule, but it would depress the condensation layer and thus increase the C_2H_6 mole fraction in the lower stratosphere, further enhancing the observed emission. However, the effect of such an abundance increase will be tempered by the sharp drop in temperature near the tropopause (see Fig. 6).

We have shown that the present observations require more ethane on Neptune than the photochemical model of Romani and Atreya (1989) derive. Colder temperatures will only increase the model–observation mismatch. Since we attempt here to test the photochemical model, we will not consider colder temperature profiles.

The preliminary analyses of Voyager 2 observations of the thermal profile of Neptune do not help constrain the profile where needed. The thermal profiles retrieved from Infrared Interferometer Spectrometer (IRIS) observations (Conrath *et al.* 1989) cover pressures greater than 10 mbar. And while the Radio Science (RSS) observations (Tyler *et al.* 1989) extend to lower pressures (~2 mbar), their thermal profiles are dependent upon the mean molecular weight which is not yet well constrained (primarily the CH_4 abundance). Their derived temperature near 2.5 mbar (their lower pressure limit) is ~20 K cooler than our nominal model indicates, and corresponds more closely to the value in the Orton *et al.* thermal profile (Fig. 2). This pressure region, however, is outside the atmospheric region which contributes to the observed line emission (see Fig. 6). The thermal profile retrieved from Voyager 2 UVS measurements (Broadfoot *et al.* 1989) covers only the very low pressure region (<0.1 mbar). They retrieve a temperature of 150 K between 1 and 100 μbar. At 0.1 mbar their temperature is ~5 K warmer than our nominal profile. Although these pressures overlap the region of ethane line formation, they correspond to the upper wing of the contribution function (see Fig. 6), and small temperature differences in that region would have little effect on our retrievals.

We used two different temperature pro-

files (Fig. 2) in fitting the different mixing ratio profiles (constant mole fraction vs photochemical model results, Fig. 1). Comparing the two temperature profiles indicates that they are not significantly different and cannot greatly affect the retrieved results. As can be seen in Fig. 2, in the line formation region, the nominal profile used with the photochemical models is within 2 K of the temperature profile used in Orton *et al.* (1987). At pressures greater than ~2 mbar, our profile is significantly warmer, but there is little contribution to the C_2H_6 line from this region of the atmosphere (see Fig. 6).

Appleby (1986) does give a range of theoretically derived temperature profiles, one of which (as mentioned previously), profile c in Fig. 5 of that reference, is about 10 K warmer than our nominal profile. Other profiles given are much colder (~50K colder) at pressures below 2 mbar.

Attempts to fit our measurements to the various ethane mixing profiles were made using a temperature profile where the temperature was increased in the 6 to 0.03 mbar region. For an increase of 10 K the best fit for the $K = 10^5$ model retrieved a mole fraction profile within a factor of 1.3 of the model, which is within our 30% retrieval uncertainty. The $K = 10^6$ mixing profile model also showed some improvement (2.3 times model) but, as before, the agreement was poorer than with the $K = 10^5$ case. The temperature profile which yielded the best agreement with the $K = 10^5$ mixing profile model was 15 K warmer in the 6–0.03 mbar region than our nominal profile (Fig. 2). Assuming this to be the "best" temperature profile, the temperature spread for a 1σ uncertainty in the resultant mixing ratio profile is 10 to 23 K warmer than our nominal temperature profile. Therefore, to reconcile the differences between the results from the photochemical model and the present measurements either the temperature must be increased to ~15 K above the nominal model for Neptune or the ethane abundance must be greater, as discussed earlier.

The effect of these higher temperatures on the photochemical models themselves must be considered. The photochemical models are sensitive to temperature changes through the temperature dependence of the reaction rates. The effect of changes on the order of 10 K on the photochemical models is usually not significant, but needs to be quantified. There is, however, an uncertainty with temperature within the models. This is because many of the reaction rates have been measured only at temperatures well above the range pertinent to modeling the stratosphere of Neptune (50–150 K).

Methane abundance. The photochemical models are also dependent upon the CH_4 abundance. However, varying the CH_4 mole fraction at the lower boundary from 0.2% to 4% in the photochemical model used here did not significantly change the resultant C_2H_6 mixing ratio profile. This is because the C_2H_6 production rate is photon, not methane, limited. Varying the mixing ratio of methane does shift the level where CH_4 photolysis takes place (to higher altitudes for larger mixing ratios). This does effect the ethane mole fraction slightly, with the trend of higher peak abundances for greater values of methane.

CONCLUSIONS

Ethane mixing profiles on Neptune were retrieved from high resolution heterodyne measurements with a cumulative uncertainty (excluding temperature profile uncertainty) of 30%. The resultant profiles were compared to previous observational results and used to test recent photochemical-condensation models. The value of the C_2H_6 mole fraction retrieved using the thermal profile and constant mixing profile model of Orton *et al.* (1987) was lower than the Orton *et al.* result, but within two of their standard deviations.

Scaling the mixing profiles derived from the theoretical model of Romani and Atreya (1989) to fit our data required 2.0 to 5.8 times more ethane in the ~0.02–2 mbar pressure region than predicted, depending on the pro-

file used. Better agreement is obtained for the lower eddy diffusion coefficient (K = 10^5 cm^2 sec^{-1}) profile. Lower eddy mixing in the lower stratosphere and higher temperatures (>10 K higher) at altitudes above the 6-mbar level can reconcile the discrepancies.

As always, the accuracies of the C_2H_6 mixing profile retrievals are limited by the input parameters, primarily the atmospheric model. The accuracy of our intensity calibration, and knowledge of the molecular line intensities, the beam profile, and rotational broadening contribute a total of about 21% uncertainty. As was seen, the atmospheric model variations can account for factors greater than 2. Hopefully, further analysis of Voyager 2 results will provide improved atmospheric parameters (i.e., temperatures) and also information on acetylene and perhaps even ethane on Neptune, which will help to further constrain and improve the existing photochemical models for Neptune.

ACKNOWLEDGMENTS

We thank James Faris, Howard Huffman, and James Guthrie for their technical support in upgrading the heterodyne spectrometer and for providing invaluable logistical support. We also acknowledge the contribution of Paul Rozmarynowski, who provided graphics support, and the IRTF telescope operators and mountain support personnel, who always do their best to make every observing run a success. This work was supported by the NASA Solar System Exploration Division, Planetary Astronomy Program. PNR acknowledges support from NASA contract NAS5-30134 at GSFC.

REFERENCES

APPLEBY, J. F. 1986. Radiative–convective equilibrium models of Uranus and Neptune. *Icarus* **65,** 383.

BROADFOOT, A. L., S. K. ATREYA, J. L. BERTAUX, J. E. BLAMONT, A. J. DESSLER, T. M. DONAHUE, W. T. FORRESTER, D. T. HALL, F. HERBERT, J. B. HOLBERG, D. M. HUNTEN, V. A. KRASNOPOLSKY, S. LINICK, J. I. LUNINE, J. C. MCCONNELL, H. W. MOOS, B. R. SANDEL, N. M. SCHEIDER, D. E. SHEMANSKY, G. R. SMITH, D. F. STROBEL, R. V. YELLE 1989. Ultraviolet spectrometer observations of Neptune and Triton. *Science* **246,** 1459–1466.

CONRATH, B., F. M. FLASAR, R. HANEL, V. KUNDE, W. MAGUIRE, J. PEARL, J. PIRRAGILA, R. SAMUELSON, P. GIERASCH, A. WEIR, B. BEZARD, D. GAUTIER, D. CRUIKSHANK, L. HORN, R. SPRINGER, W. SHAFFER 1989. Infrared observations of the Neptunian system. *Science* **246,** 1454–1459.

DAUNT, S. J., A. K. ATAKAN, W. E. BLASS, G. W. HALSEY, D. E. JENNINGS, D. C. REUTER, J. SUSSKIND, AND J. W. BRAULT 1984. The 12 micron band of ethane: High-resolution laboratory analysis with candidate lines for infrared heterodyne searches. *Astrophys. J.* **280,** 921–936; also Atakan, A. K., W. E. Blass, J. W. Brault, S. J. Daunt, G. W. Halsey, D. E. Jennings, D. C. Reuter, and J. Susskind 1983. *The 12 Micron Band of Ethane: A Spectral Catalog from 765 cm^{-1}-900 cm^{-1}.* NASA/GSFC Technical Memorandum 85108.

GILLETT, F. C., AND G. H. RIEKE 1977. 5–20 micron observations of Uranus and Neptune. *Astrophys. J.* **218,** L141.

HAMMEL, H. B. 1989. Neptune cloud structure at visible wavelengths. *Science* **244,** 1165–1167.

KOSTIUK, T., AND M. J. MUMMA 1983. Remote sensing by IR heterodyne spectroscopy. *Appl. Opt.* **17,** 2644.

KOSTIUK, T., M. J. MUMMA, F. ESPENAK, D. DEMING, D. E. JENNINGS, W. MAGUIRE, AND D. ZIPOY 1983. Measurements of stratospheric ethane in the Jovian south polar region from infrared heterodyne spectroscopy of the ν9 band near 12 microns. *Astrophys. J.* **265,** 564.

KOSTIUK, T., F. ESPENAK, M. J. MUMMA, D. DEMING, AND D. ZIPOY 1987. Variability of ethane on Jupiter. *Icarus* **72,** 394.

KOSTIUK, T., F. ESPENAK, M. J. MUMMA, AND P. ROMANI 1989. Infrared studies of hydrocarbons on Jupiter. *Infrared Phys.* **29,** 199.

MACY, W., JR., AND W. SINTON 1977. Detection of methane and ethane emission on Neptune but not Uranus. *Astrophys. J.* **218,** L79.

MACY, W., JR. 1980. Mixing ratios of methane, ethane, and acetylene in Neptune's stratosphere. *Icarus* **41,** 153.

ORTON, G. S., A. T. TOKUNAGA, AND J. CALDWELL 1983. Observational constraints on the atmospheres of Uranus and Neptune from new measurements near 10 μm. *Icarus* **56,** 147.

ORTON, G. S., D. K. AITKEN, C. SMITH, P. F. ROCHE, J. CALDWELL, AND R. SNYDER 1987. The spectra of Uranus and Neptune at 8–14 and 17–23 μm. *Icarus* **70,** 1–12.

ORTON, G. S., K. H. BAINES, J. CALDWELL, P. N. ROMANI, A. T. TOKUNAGA, AND R. A. WEST, 1990. Calibration of the 7- to 14-μm brightness spectra of Uranus and Neptune. *Icarus* **85,** 257–265.

ROMANI, P. N., AND S. K. ATREYA 1989. Stratospheric aerosols from CH_4 photochemistry on Neptune. *Geophys. Res. Lett.* **16,** 941–944.

ROMANI, P. N., AND S. K. ATREYA 1988. Methane photochemistry and haze production on Neptune. *Icarus* **74,** 424.

SMITH, B. A., L. A. SODERBLOM, D. BANFIELD, C. BARNET, A. T. BASILEVSKY, R. F. BEEBE, K. BOLLINGER, J. M. BOYCE, A. BRAHIC, G. A. BRIGGS, R. H. BROWN, C. CHYBA, S. A. COLLINS, T. COLVIN, A. F. COOK II, D. CRISP, S. K. CROFT, D. CRUIKSHANK, J. N. CUZZI, G. E. DANIELSON, M. E. DAVIES, E. DE JONG, L. DONES, D. GODFREY, J. GOGUEN, I. GRENIER, V. R. HAEMMERLE, H. HAMMEL, C. J. HANSEN, C. P. HELFENSTEIN, C. HOWELL, G. E. HUNT, A. P. INGERSOLL, T. V. JOHNSON, J. KARGEL, R. KIRK, D. I. KUEHN, S. LIMAYE, H. MASURSKY, A. MCEWEN, D. MORRISON, T. OWEN, W. OWEN, J. B. POLLACK, C. C. PORCO, K. RAGES, P. ROGERS, D. RUDY, C. SAGEN, J. SCHWARTZ, E. M. SHOEMAKER, M. SHOWALTER, B. SICARDY, D. SIMONELLI, J. SPENCER, L. A. SMOROWSKY, C. STOKER, R. G. STROM, V. E. SUOMI, S. P. SYNOTT, R. J. TERRILE, P. THOMAS, W. R. THOMSON, A. VERBISCER, J. VEVERKA 1989. Voyager 2 at Neptune: Imaging science results. *Science* **246,** 1422–1449.

SUSSKIND J., D. REUTER, D. E. JENNINGS, S. J. DAUNT, W. E. BLASS, AND G. W. HALSEY 1982. Diode laser spectra of the torsional splitting in the $\nu 9$ band of ethane: Torsion–vibration–rotation interactions and the barrier to internal rotation. *J. Chem. Phys.* **77,** 2728.

TOKUNAGA, A. T., G. S. ORTON, AND J. CALDWELL 1983. New observational constraints on the temperature inversions of Uranus and Neptune. *Icarus* **53,** 141–146.

TYLER, G. L., D. N. SWEETNAM, J. D. ANDERSON, S. E. BORUTZKI, J. K. CAMPBELL, V. R. ESHLEMAN, D. L. GRESH, E. M. GURROLA, D. P. HINSON, N. KAWSHIMA, E. R. KURSINSKI, G. S. LEVY, G. F. LINDAL, J. R. LYONS, E. A. MAROUF, P. A. ROSEN, R. A. SIMPSON, G. E. WOOD 1989. Voyager radio science observations of Neptune and Triton. *Science* **246,** 1466–1473.

WARWICK, J. W., D. R. EVANS, G. R. PELTZER, R. G. PELTZER, J. H. ROMIG, C. B. SAWYER, A. C. RIDDLE, A. E. SCHWEITZER, M. D. DESCH, M. L. KAISER, W. M. FARELL, T. D. CARR, I. DE PATER, D. H. STAELIN, S. GULKIS, R. L. POYNTER, A. BOISCHOT, F. GENOVA, Y. LEBLAND, A. LECACHEUX, B. M. PEDERSEN, P. ZARKA 1989. Voyager planetary radio astronomy at Neptune. *Science* **246,** 1498–1501.